JOURNAL OF Materials CHEMISTRY

Nanocrystalline rare earth stabilized zirconia: solvothermal synthesis *via* heterogeneous nucleation-growth mechanism, and electrical properties

Yawen Zhang, Gang Xu, Zhengguang Yan, Yu Yang, Chunsheng Liao and Chunhua Yan*

State Key Laboratory of Rare Earth Materials Chemistry and Applications, PKU-HKU Joint Laboratory in Rare Earth Materials and Bioinorganic Chemistry, College of Chemistry and Molecular Engineering, Peking University, Beijing 100871, China.
E-mail: chyan@chem.pku.edu.cn; Fax: +86-10-6275-4179

Received 5th October 2001, Accepted 5th February 2002
First published as an Advance Article on the web 4th March 2002

Homogeneous nanocrystalline $(ZrO_2)_{0.92}(RE_2O_3)_{0.08}$ (RE = Y, Sc) with large specific surface areas and cubic structure were solvothermally synthesized from the urea coprecipitated (Zr,RE)-hydroxide gel or the gel-calcined oxide in water (or absolute ethanol) under mild conditions. Both the hydroxide and the oxide powders showed very high solvothermal reactivity. Mainly by X-ray diffraction and transmission electron microscopy, the solvothermal mechanism was explored. The heterogeneous nucleation-growth, *i.e.* an *in situ* transformation of hydrous (Zr,RE)-oxide with an ordered cubic structure *via* dissolution and recrystallization is supposed to predominately account for the nanocrystalline crystallization. The as-obtained nanocrystallite exhibited a good sinterability. Over the temperature range of 360–600 °C, nanocrystalline $(ZrO_2)_{0.92}(Y_2O_3)_{0.08}$ displayed enhanced specific grain boundary conductivity due to the size-dependent grain boundary impurity segregation.

Introduction

Zirconia-based ceramics are receiving intensive attention for their applications in solid oxide fuel cells (SOFCs), oxygen sensors and transformation-toughened materials. Using fine particles is regarded as a promising way to improve the homogeneity and sinterability of the green body and finally to achieve the desirable properties for the applications. So far, various techniques including inert gas condensation,[1] plasma technique,[2] spray pyrolysis,[3] coprecipitation,[4] sol–gel synthesis,[5] forced hydrolysis,[6] and solvothermal (hydrothermal[7–10] and alcohol–thermal[11]) methods have been developed to prepare the fine particles. Among these techniques, the solvothermal method promises a single step low-temperature synthesis, superior composition and morphological control, and powder reactivity.

More recently, the electrical properties of nanostructured oxide ion conductors such as $(ZrO_2)_{0.92}(Y_2O_3)_{0.08}$ (8YZr) and $(ZrO_2)_{0.92}(Sc_2O_3)_{0.08}$ (8ScZr) (as good candidate electrolytes for SOFCs) has stimulated increased interest.[12–14] In order to clarify the nature of the ionic conduction in bulk stabilized ZrO_2, well-controlled nanostructures are required and these can be obtained by various synthesis techniques. In this work, the solvothermal synthesis and electrical properties of nanostructured $(ZrO_2)_{0.92}(RE_2O_3)_{0.08}$ (RE = Y, Sc) have been investigated.

Previously, some researchers have reported the solvothermal conditions required for synthesizing zirconia sols and yttria-stabilized zirconia (YSZ).[8–11,15,16] For instance, Zhao *et al.* synthesized stable cubic nanocrystalline zirconia sols by alcohol–thermal synthesis.[11] Lin and Duh[15] showed that nanoparticulate $(ZrO_2)_{0.925}(CeO_2)_{0.055}(YO_{1.5})_{0.02}$ of tetragonal structure could be prepared by a combination of urea coprecipitation and subsequent hydrothermal treatment at pH 10.8; Dell'Agli and Mascolo[16] employed zirconia gel and microcrystalline Y_2O_3 as starting materials to synthesize ultrafine YSZ powders by hydrothermal treatment at 110 °C in the presence of the mineralizer Na_2CO_3. These studies proved that solvothermal synthesis is extremely effective in making ultrafine and weakly agglomerated zirconia materials, although the phase composition strongly depends on the crystallization conditions and mechanism. Up to now, there has been no report about the solvothermal synthesis of scandia-stabilized zirconia (ScSZ). On the other hand, investigations into the solvothermal mechanism are still inadequate. In order to screen the synthetic conditions required for making powders with well-defined properties, there is a further need for using various characterization techniques to explore the solvothermal mechanism and the nature of the solution species.

The aims of this work are to investigate the solvothermal synthesis of nanocrystalline $(ZrO_2)_{0.92}(RE_2O_3)_{0.08}$ under mild conditions in water or absolute ethanol, using urea coprecipitated hydroxide gel or the gel-calcined oxide powder as starting materials, to make clear the solvothermal mechanism, and to examine the electrical properties of the nanocrystallite. To our knowledge, the solvothermal reactivity of the gel-calcined oxide is studied here for the first time. The solvothermal products were characterized by thermogravimetry and differential thermal analysis (TG-DTA), X-ray diffraction (XRD), scanning electron microscopy (SEM), high-resolution transmission electron microscopy (HRTEM), BET surface area analysis, and impedance spectroscopy. In this paper, the solvothermal synthesis (including the mechanism) and the electrical properties of nanocrystalline $(ZrO_2)_{0.92}(RE_2O_3)_{0.08}$ are presented.

Experimental

Preparation

Quantitative solutions of $ZrO(NO_3)_2$ (AR), $RE(NO_3)_3$ (AR, >99.95%) and urea (AR) in the molar ratio of ZrO^{2+} : RE^{3+} : urea = 0.85 : 0.15 : 30, were employed to prepare the stock solution with a cation concentration of 0.15 mol L^{-1}.

 DOI: 10.1039/b109091g

After hydrolysis at 90 °C for 48 h in a closed system in a water bath, white hydroxide gel was formed from the stock solution at pH 9. The gel was washed with doubly distilled water and pure ethanol to remove ionic impurities, and finally treated by freeze drying in *tert*-butyl alcohol. A Teflon cup (100 mL) filled with a doubly distilled water (or absolute ethanol, 1 mol L^{-1} NaOH in absolute ethanol, 9 mol L^{-1} NaOH solution) suspension (60 mL) of the hydroxide gel (180 mg), or the gel-calcined oxide powder (calcined at 300 °C for 1 h; 100–300 mg) was placed in a stainless-steel autoclave. The solvothermal treatment was performed at 120–180 °C for 1–7 days under autogenous pressure in an electric oven. As the autoclave cooled down to room temperature, the product was collected, washed with doubly distilled water and then ethanol several times, and then dried at 60 °C.

The dried products were calcined at 800 °C for 2 h so as to test their calcination behavior. In order to prepare dense specimens, the products (~0.3 g) were uniaxially pressed into tablets with a diameter of 5 mm under 12 MPa pressure. The tablets were then sintered at 1000 °C for 8 h under still air in a muffle furnace. The nomenclature and preparative conditions for some typical samples are listed in Table 1.

Characterization methods

The thermal behavior was investigated with a thermal analyzer (Du Pont 2100) in air at a heating rate of 10 °C min^{-1}, using α-Al_2O_3 as a reference. The crystal structures were identified by a powder X-ray diffractometer (Rigaku D/max-2000), employing Cu-Kα radiation (λ = 1.5408 Å). The lattice parameters were calculated using the LAPOD software, which uses least-squares refinement of the cell dimensions obtained from the powder data by Cohen's method.[17,18] The average grain size D was estimated according to the Scherrer equation,[19]

$$D = 0.90\lambda/\cos\theta$$

where θ is the diffraction angle of the (111) peak, β is the full width at half maximum (FWHM) of the (111) peak (in radian), which is calibrated from high purity silicon. The percentage of monoclinic phase was calculated from the relative peak area of the monoclinic (m) peaks $(1\ 1\ -1)_m+(1\ 1\ 1)_m$ and the monoclinic plus cubic (c) peaks $(1\ 1\ -1)_m+(1\ 1\ 1)_m+(1\ 1\ 1)_c$. The BET specific surface area S_{BET} was measured by nitrogen physisorption at 77.5 K using an ASAP 2010 analyzer (Micromeritics Co. Ltd.). Nanoparticle morphologies and stoichiometry were examined by TEM coupled with energy dispersive X-ray analysis (EDAX) at a resolution of 159 eV (TEM, 200CX, JEOL; HRTEM, H-9000, Hitachi). The statistical error of the EDAX system used was about 5–10%. The surface micrographs were taken by SEM (AMARY 1910FE).

Electrical property measurements

The electrical properties of the dense specimens were determined in air by ac two-probe measurements on a frequency response analyzer (HP4192A LF, 200 Hz–12 MHz).[20] The impedance data points were collected twice with a temperature interval of 40 °C on cooling over the temperature range of 800–360 °C. Two Pt lead wire electrodes were attached to the two terminals of the specimen with Pt paste, which was fired at 950 °C for 30 min to remove the polymeric components. The electrical conductivity was calculated from the interceptions of the observed semicircle on the real axis of a Cole–Cole plot.

Results and discussion

Synthesis and mechanism

Previously, urea precipitation was thought to be very effective in making weakly-agglomerated ultrafine powders *via* the homogeneous hydrolysis of cations, under a constant pH value yielded by a fixed concentration of urea.[21–23] Thus in this work, during the synthesis of (Zr,Y)-hydroxide gel by the above-mentioned method, ZrO^{2+} and Y^{3+} ions are expected to hydrolyze simultaneously at pH 9 and possibly form complexes with OH^- ions and/or H_2O molecules, such as $[Zr(OH)_5]^-$ and $Y(OH)_4^-$,[24,25] which may transform into polymeric complexes (trimeric and/or tetrameric).[24,25] Upon aging, further polymerization between the Zr and Y species is likely to occur *via* –OH bridging during structural rearrangement, and finally this could lead to the formation of an ordered structure by the dehydration of the surface hydroxyl of the precipitated crystallite (at 90 °C for 48 h). The overall reactions can be formulated as follows:

$$CO(NH_2)_2 + 3H_2O \rightarrow CO_2 + 2NH_4^+ + 2OH^-$$

$$ZrO(NO_3)_2 + Y(NO_3)_3 + OH^- \rightarrow \text{(Zr,Y)-hydroxide}$$

Fig. 1 shows a combined TG-DTA run of the (Zr,Y)-hydroxide gel. It should be noted that the gel can dehydrate nearly completely below 300 °C, while displaying a small endothermic (endo.) effect at *ca.* 200 °C. However, no obvious exothermic (exo.) peak for the transition from amorphous to crystalline within the temperature range of 400–500 °C was detected. Therefore, it was considered that the hydrolysis products have already crystallized to some extent.[23] After calcining at 300 °C for 1 h, the (Zr,Y)-hydroxide gel has become coarse-grained anhydrous oxide powder. Fig. 2

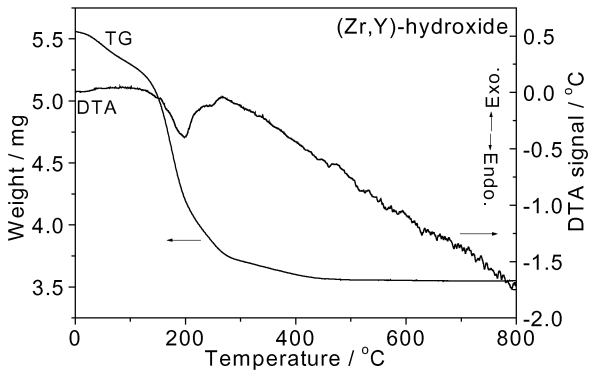

Fig. 1 A combined TG-DTA run of (Zr,Y)-hydroxide gel.

Table 1 Nomenclature and preparative conditions of some typical samples

	Starting material	Reaction system	Reactant mass/mg
8YZr-1	(Zr,Y)-hydroxide	Water	180
8YZr-2	(Zr,Y)-hydroxide	1 mol L^{-1} NaOH–ethanol	180
8YZr-3	(Zr,Y)-oxide	Water	100
8YZr-4	(Zr,Y)-oxide	1 mol L^{-1} NaOH–ethanol	100
8ScZr-1	(Zr,Sc)-hydroxide	Water	180
8ScZr-2	(Zr,Sc)-hydroxide	1 mol L^{-1} NaOH–ethanol	180
8ScZr-3	(Zr,Sc)-oxide	Water	100
8ScZr-4	(Zr,Sc)-oxide	1 mol L^{-1} NaOH–ethanol	100

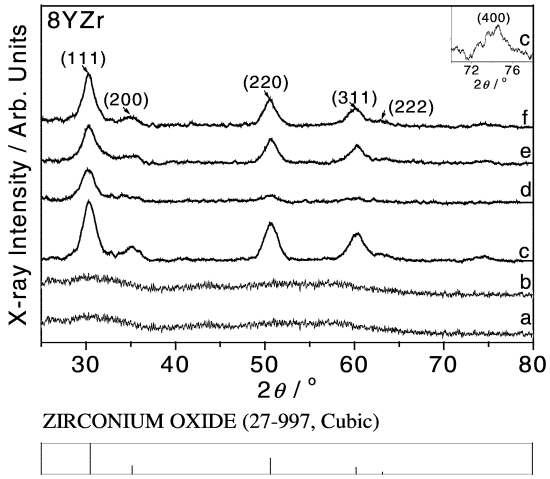

Fig. 2 XRD patterns for (a) (Zr,Y)-hydroxide gel, (b) (Zr,Y)-oxide, (c) 8YZr-1, (d) 8YZr-2, (e) 8YZr-3 and (f) 8YZr-4 over the 2θ range of 25–80°. The inset is a scale-enlarged profile for 8YZr-1 over 70–78°.

exhibits the XRD patterns of the (Zr,Y)-hydroxide gel, the (Zr,Y)-oxide and the as-synthesized 8YZr products. A weak broad peak around 30° is observed for the (Zr,Y)-hydroxide gel (Fig. 2a), even after calcining at 300 °C (Fig. 2b). Therefore, it is further argued that the (Zr,Y)-hydroxide gel may exist in the form of hydrous oxide with an ordered structure, rather than as a hydroxide with an amorphous structure. Such an ordered structure, similar to cubic, might be the result of the long period of aging at 90 °C during urea coprecipitation, and it was also suggested by Tsukada *et al.*[24] when synthesizing YSZ by hydrothermal synthesis. Accordingly, it is possible for the hydrous (Zr,Y)-oxide to crystallize into nanocrystalline $(ZrO_2)_{0.92}(Y_2O_3)_{0.08}$ *via* heterogeneous nucleation-growth (*in situ* transformation mechanism) under solvothermal conditions.[24]

The reaction time (1–7 days) and temperature (120–180 °C) for the solvothermal reaction were screened by XRD and TEM analysis. The experimental results showed that both elevating the reaction temperature and extending the reaction time could help in the crystallization of 8YZr. So in the following solvothermal treatment, the reaction time and temperature were fixed at 3 days and 180 °C, respectively, for convenience in comparing the experimental results.

The broadening of the XRD diffraction lines in Fig. 2c–2f indicates the nanocrystalline formation after solvothermal treatment. It should also be observed that cubic nanocrystalline 8YZr can be solvothermally obtained either in water or 1 mol L^{-1} NaOH–ethanol systems, no matter whether the (Zr,Y)-hydroxide gel or the gel-calcined powders were adopted as the starting materials (inset in Fig. 2).[26] The as-obtained (Zr,Y)-hydroxide gel and (Zr,Y)-oxide powder exhibited distinctly high solvothermal reactivity.

The intensity of the (111) peak in Fig. 2 reflects the difference in crystallization for the resultant nanocrystalline 8YZr. With the (Zr,Y)-hydroxide gel as starting material, it seemed easier crystallizing in water than in ethanol, because the water system can supply sufficient water for the crystallization; whereas, when the (Zr,Y)-oxide was employed, it appeared that better crystallizing occurred in ethanol than in water, possibly because ethanol could effectively break up the agglomerates in the (Zr,Y)-oxide, and thus accelerate the solvothermal reaction.

TEM observations revealed that the products derived from the (Zr,Y)-oxide showed more agglomerates than these derived from the (Zr,Y)-hydroxide. Hence, Fig. 3 only gives the TEM micrographs of the products derived from the (Zr,Y)-hydroxide in water (8YZr-1, Fig. 3a) and in 1 mol L^{-1} NaOH–ethanol (8YZr-2, Fig. 3b), respectively. The primary particles of nanocrystalline $(ZrO_2)_{0.92}(Y_2O_3)_{0.08}$ of cubic structure are

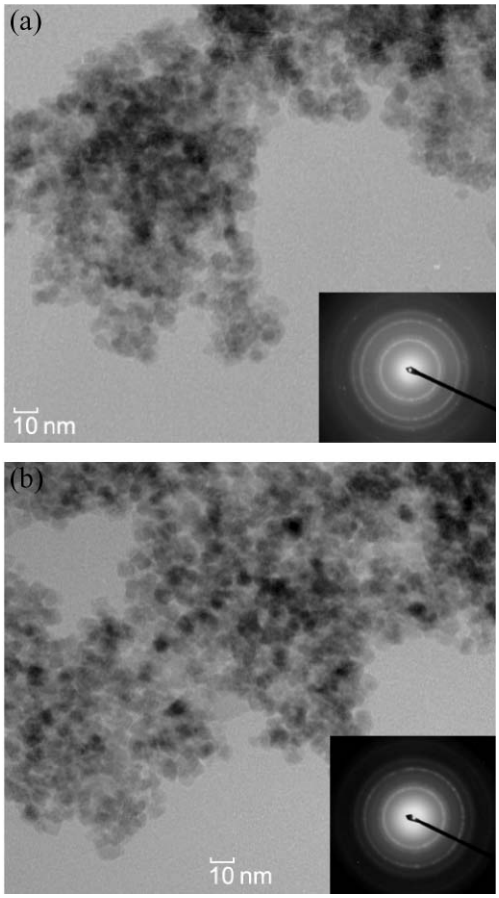

Fig. 3 TEM micrographs and electron diffraction patterns (insets) of (a) 8YZr-1 and (b) 8YZr-2.

noticed to have a size of 5–8 nm, be homogenous with well-defined edges, and in loose clumps with soft contacts.

In order to further confirm the *in situ* transformation mechanism responsible for the formation of nanocrystalline 8YZr, some crystallization experiments were carried out. With the (Zr,Y)-oxide as the reactant, the XRD profile of the derived product (Fig. 4a) was nearly the same as that of the (Zr,Y)-oxide (Fig. 2b). This result means that no crystallization occurred in absolute ethanol. On the other hand, a sample appeared of poor crystallization (Fig. 4b), when the (Zr,Y)-hydroxide gel was used and only a little water was supplied by the ethanol system. Obviously, the presence of adequate water is critical in dissolving the oxide powder into hydrous oxide for full crystallization. Because the reversible reaction between NaOH and C_2H_5OH under solvothermal conditions could result in enough water and a strong basic environment, the crystallization of 8YZr-2 and 8YZr-4 was catalyzed. Consequently, 8YZr-2 (Fig. 2d) and 8YZr-4 (Fig. 2f) like 8YZr-1 (Fig. 2c) and 8YZr-3 (Fig. 2e) attained full crystallization, which was evidenced by the lack of a small exothermic peak at about 430 °C favored for the uncrystallized zirconia gel (Fig. 5).[27]

As is seen from Fig. 4c, 23.2% monoclinic phase was formed after hydrothermal treatment, when increasing the reactant mass of the (Zr,Y)-oxide from 100 to 300 mg. This indicates that the as-proposed ordered structure is metastable in nature, it allowed the (Zr,Y)-oxide partially to precipitate and crystallize into *m*-ZrO_2 and hexagonal $Y(OH)_3$ during hydrothermal reaction. Dell'Agli and Mascolo[16] found the structural rearrangement of zirconia gel could be greatly accelerated in the presence of NaOH. Thus, the monoclinic transformation can be suppressed by the addition of NaOH to our reaction system. A 9 mol L^{-1} NaOH solution was used, the derived product was yielded in a pure cubic structure (Fig. 4d). These

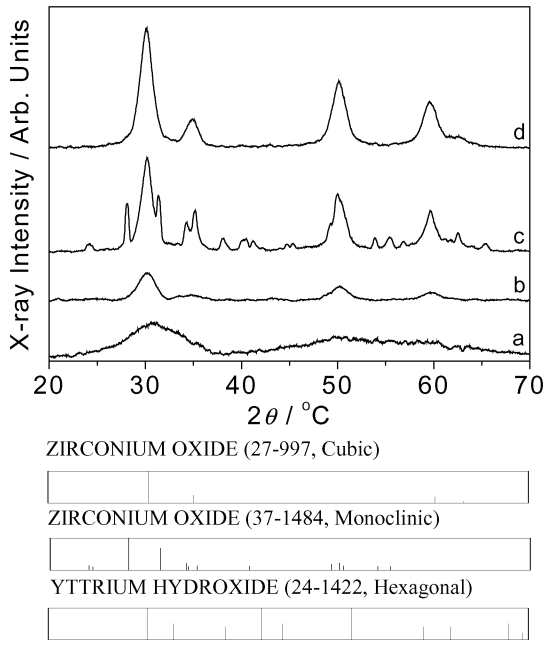

Fig. 4 XRD patterns for the products after solvothermal treatment at 180 °C for 3 days. (a)100 mg (Zr,Y)-oxide in ethanol, (b) 180 mg (Zr,Y)-hydroxide in ethanol, (c) 300 mg (Zr,Y)-oxide in water and (d) 300 mg (Zr,Y)-oxide in 9 mol L^{-1} NaOH solution.

findings suppose that, here, homogeneous nucleation-growth (dissolution–precipitation mechanism) was working as well, when the *in situ* transformation mechanism dominates the solvothermal crystallization.

The above solvothermal reactions can be summarized by Scheme 1, in which, (a) and (s) represent the aqueous and solid phases, respectively, and *n* denotes the molar number of water molecules. During the nanocrystalline crystallization, the starting materials must be firstly dissolved in water to become $[(Zr,Y)\text{-oxide}\cdot nH_2O]_{(a)}$ with an ordered structure, subsequently, the hydrous oxide *in situ* transforms into anhydrous $(ZrO_2)_{0.92}(Y_2O_3)_{0.08}$ (the limiting step), and achieves full crystallization *via* dissolution–recrystallization.

Fig. 6 depicts the HRTEM micrographs of the (Zr,Y)-hydroxide gel (inset is the pattern of selected area electron diffraction), and nanocrystalline 8YZr-1, 8YZr-2 and 8YZr-3. The weak electron diffraction generated by the hydroxide particles of less than 10 nm with blur brims presumes the existence of nuclei for *in situ* transformation (Fig. 6a). The primary particles of nanocrystalline $(ZrO_2)_{0.92}(Y_2O_3)_{0.08}$ are observed to be homogenous with well-defined edges, discrete with little necks between grains (Fig. 6b–d). Therefore, the

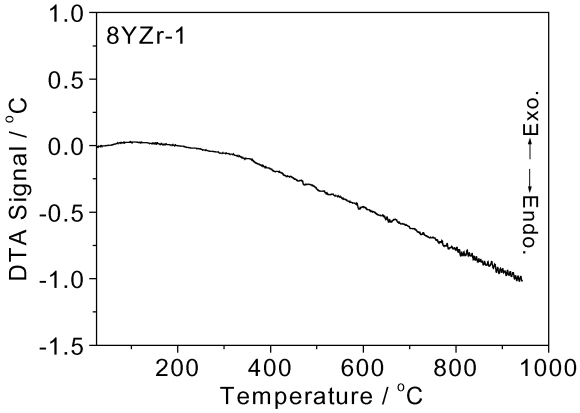

Fig. 5 DTA curve of 8YZr-1 solvothermally synthesized from 180 mg (Zr,Y)-hydroxide in water at 180 °C for 3 days.

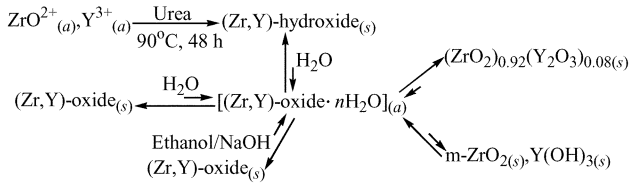

Scheme 1

morphological observations strongly support the *in situ* transformation mechanism.[28]

As is described in Fig. 7, the XRD patterns of the (Zr,Sc)-hydroxide gel, the gel-calcined oxide powder and the as-synthesized 8ScZr products strongly suggest that cubic nanocrystalline 8ScZr can also be made by the *in situ* transformation mechanism. On the other hand, the crystallizing behaviors exhibited by the (Zr,Sc)-hydroxide gel and the (Zr,Sc)-oxide powder in water or ethanol are similar to those displayed by the (Zr,Y)-hydroxide gel and the (Zr,Y)-oxide powder (see the intensity variation of the (111) peak in Fig. 7c–f and Fig. 2c–f). The nanocrystallites are uniformly of size 5–8 nm, as observed from the TEM images (Fig. 8).

The atomic concentrations of Zr and Y in 8YZr-1, and Zr and Sc in 8ScZr-1 measured by EDAX are 83.2% and 16.8%, 84.0% and 16.0%, respectively. These values basically agree with the theoretical compositions of 8YZr and 8ScZr, respectively, and hint that the ZrO^{2+} and RE^{3+} ions were completely hydrolyzed and coprecipitated after aging at 90 °C for 48 h in the presence of urea. No peak at 1.04 keV was found for elemental Na in the EDAX spectra of 8YZr-2, 8YZr-4, 8ScZr-2 and 8ScZr-4, indicating that the Na impurities in these nanocrystalline products were thoroughly washed off. The average lattice parameters of cubic nanocrystalline $(ZrO_2)_{0.92}(Y_2O_3)_{0.08}$ and $(ZrO_2)_{0.92}(Sc_2O_3)_{0.08}$ were fitted to be 5.14 and 5.09 Å, respectively, which are in good accordance with the data previously reported.[29,30]

Table 2 gives the average crystallite size and BET specific surface area of the samples. It can be seen that the average crystallite sizes of the as-obtained nanocrystalline 8YZr and 8ScZr are all in the range of 5–7 nm, consistent with those determined by TEM. Except 8ScZr-4, the other samples have a specific surface area larger than 100 $m^2\ g^{-1}$. After calcining at 800 °C for 2 h, nanocrystalline 8YZr and 8ScZr still maintain a cubic structure. However, their specific surface area percentage drops drastically, in the range from 35% to 90%, as a result of the rapid growth and severe coarsening that occurs for the nanoparticles at the elevated calcining temperature. Among the samples listed in Table 2, 8YZr-1 and 8ScZr-1 show the least reduction in the specific surface area, possibly due to the fact that they are more dispersed than the others, as found by TEM. So only their TEM micrographs are depicted in Fig. 9, from which it is noticed that nanocrystalline 8YZr-1 and 8ScZr-1 grow to about 15 and 10 nm respectively. They are homogeneous and show much brighter electron diffraction rings after calcination.

Electrical properties

In order to understand the ionic conduction in the nanocrystallites, the average crystallite size of 8YZr-1 and 8ScZr-1 should not exceed 100 nm. The experiments showed that the size requirement could be met at a sintering temperature below 1200 °C. Fig. 10 exhibits the XRD patterns of 8YZr-1 and 8ScZr-1 pellets after sintering at 1000 °C for 8 h. It should be noted that 8YZr-1 and 8ScZr-1 display a slight phase splitting, and are in a phase of a majority of cubic plus a trace of tetragonal. The average crystallite size of the 8YZr-1 and 8ScZr-1 samples are 29 and 48 nm, respectively, as calculated by the XRD line-broadening analysis. Fig. 11 shows the surface micrographs of 8YZr-1 (a) and 8ScZr-1 (b). It can be seen that

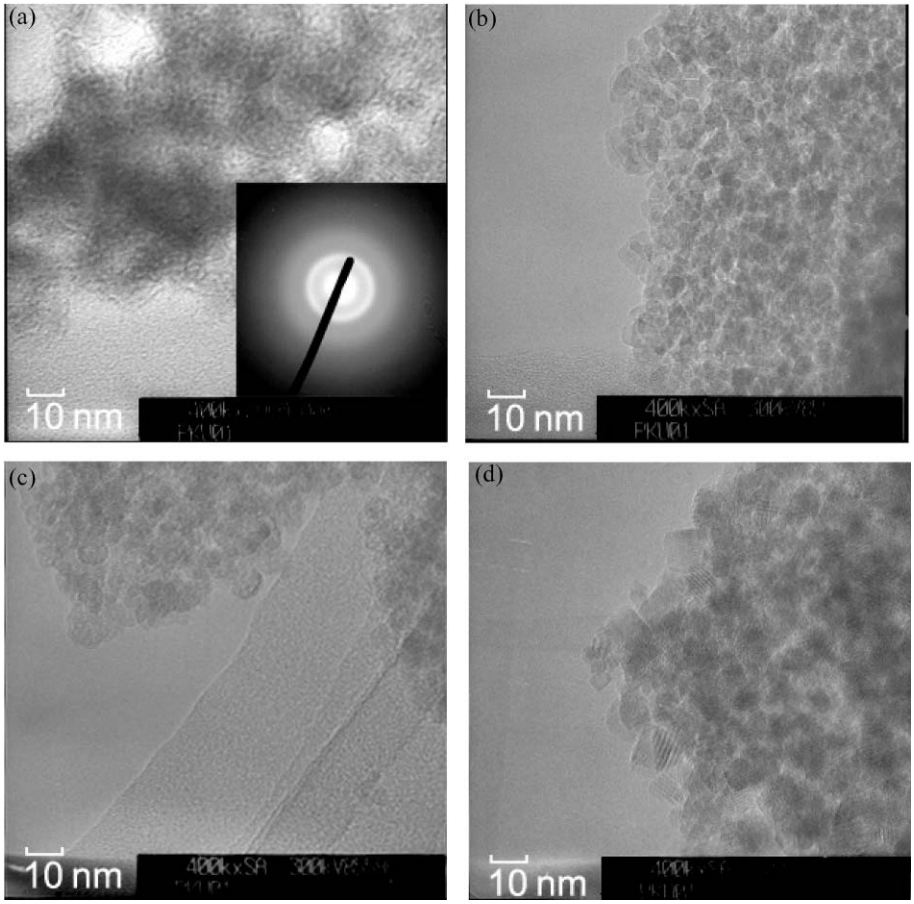

Fig. 6 HRTEM micrographs and electron diffraction pattern (inset) of the (Zr,Y)-hydroxide gel (a), and HRTEM micrographs of (b) 8YZr-1, (c) 8YZr-2 and (d) 8YZr-3.

the sintered body is highly dense and of uniform grain size, indicating that the as-synthesized nanocrystallites have a good sinterability. As was estimated from the mass and geometric dimensions of the pellets, the sintered density of 8YZr-1 and 8ScZr-1 are about 87% and 80% of the theoretical density, respectively. Therefore, 8YZr-1 is denser than 8ScZr-1, which can also be observed from Fig. 11.

Fig. 12 depicts the impedance spectra of 8YZr-1 and 8ScZr-1. At both 400 and 600 °C, there exists one semicircle at high frequency in the impedance spectra. This semicircle is ascribed to the superposition of bulk and grain boundary processes. Such superpositions are often found when the grain size is

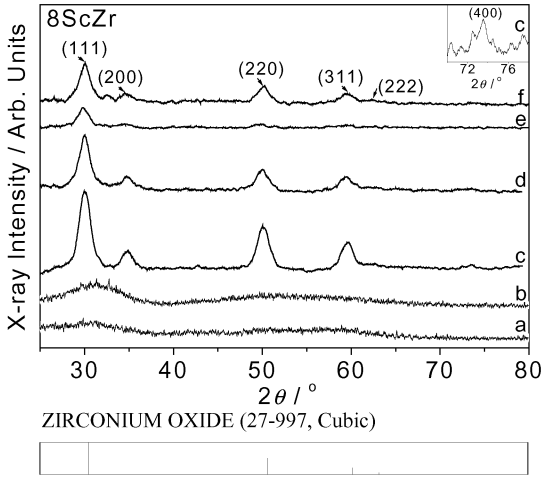

Fig. 7 XRD patterns for (a) (Zr,Sc)-hydroxide gel, (b) (Zr,Sc)-oxide, (c) 8ScZr-1, (d) 8ScZr-2, (e) 8ScZr-3 and (f) 8ScZr-4 over the 2θ range of 25–80°. The inset is a scale-enlarged profile for 8ScZr-1 over 70–78°.

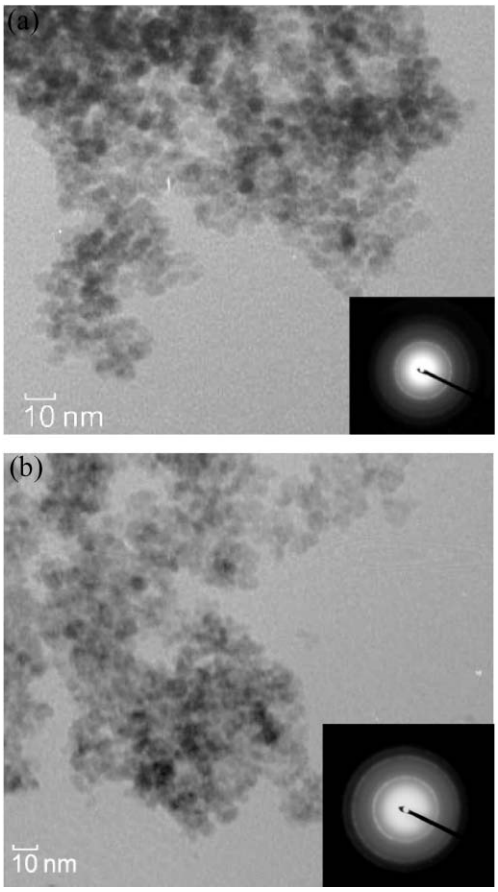

Fig. 8 TEM micrographs and electron diffraction patterns (insets) of (a) 8ScZr-1 and (b) 8ScZr-2.

Table 2 Average crystallite size and BET specific surface area of $(ZrO_2)_{0.92}(RE_2O_3)_{0.08}$ (RE = Sc, Y) nanocrystallites solvothermally synthesized at 180 °C for 3 days

	8YZr-1	8YZr-2	8YZr-3	8YZr-4	8ScZr-1	8ScZr-2	8ScZr-3	8ScZr-4
D/nm	6.5	6.5	6.7	6.4	6.0	5.5	5.0	5.9
S_{BET}/m^2 g^{-1}	176	186	150	160	194	208	105	57.2
S_{BET}[a]/m^2 g^{-1}[a]	112	64	97	83	98	83	36	6.2

[a]After calcining at 800 °C for 2 h.

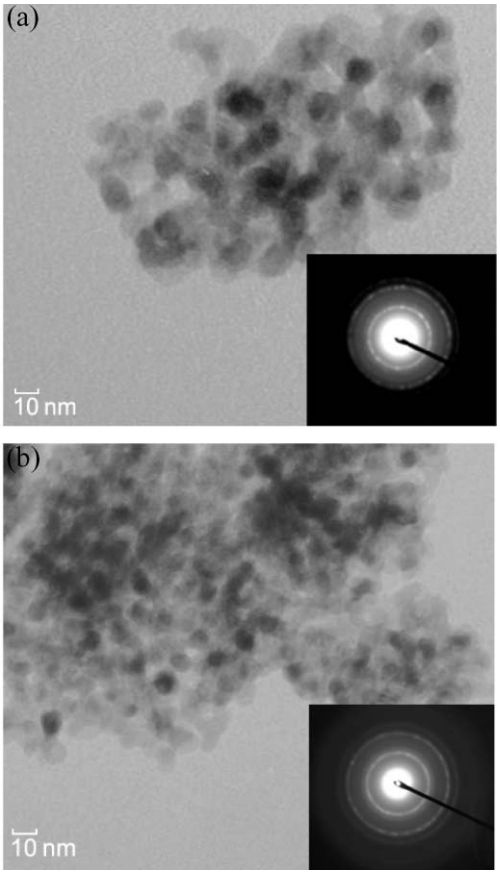

Fig. 9 TEM micrographs and electron diffraction patterns (insets) of (a) 8YZr-1 and (b) 8ScZr-1 after calcining at 800 °C for 2 h.

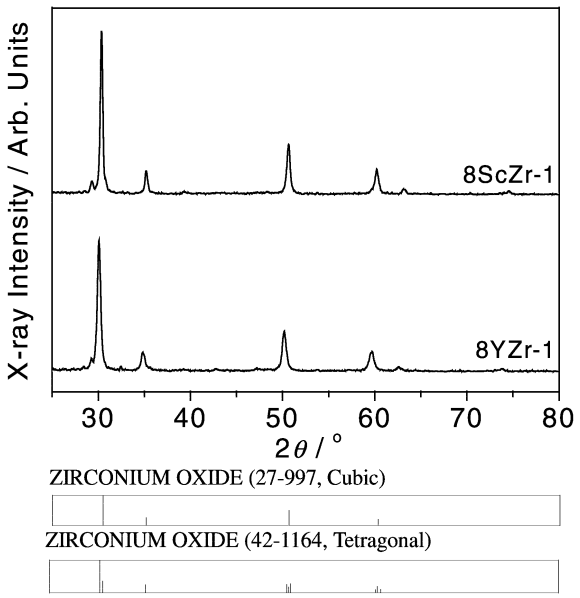

Fig. 10 XRD patterns for nanocrystalline 8YZr-1 and 8ScZr-1 after sintering at 1000 °C for 8 h.

reduced from μm to nm.[12–14] At 400 °C, the capacitance values for 8YZr-1 and 8ScZr-1 were determined to be 1.7×10^{-10} and 2.5×10^{-11} F, respectively; and at 600 °C, they were 1.7×10^{-10} and 2.7×10^{-11} F, respectively. These results strongly suggest that the semicircle and its associated resistance are governed by the grain boundary properties of the nanocrystallite.[31] At 600 °C, the impedance at low frequency (<25 kHz) in the impedance spectrum of 8ScZr-1 is ascribed to the electrode contact.[20]

The impedance spectra of the nanocrystallites show considerable differences from those of the microcrystallites. At low temperature, three semicircles corresponding to bulk resistance

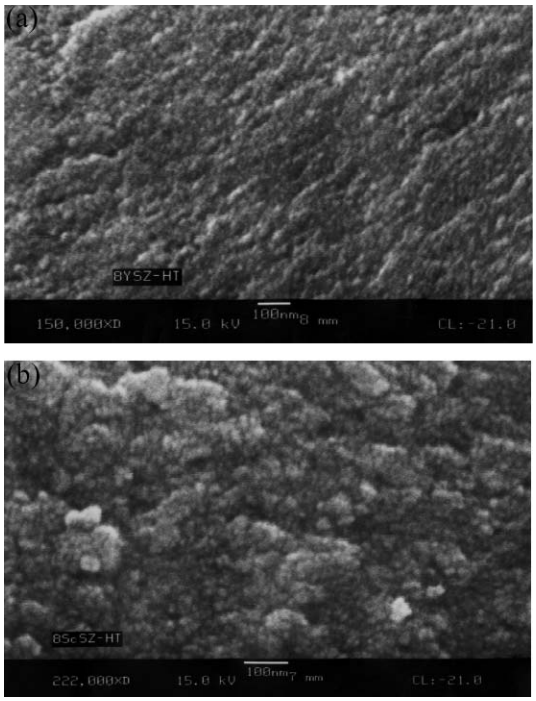

Fig. 11 Surface SEM micrographs of nanocrystalline (a) 8YZr-1 and (b) 8ScZr-1 after sintering at 1000 °C for 8 h.

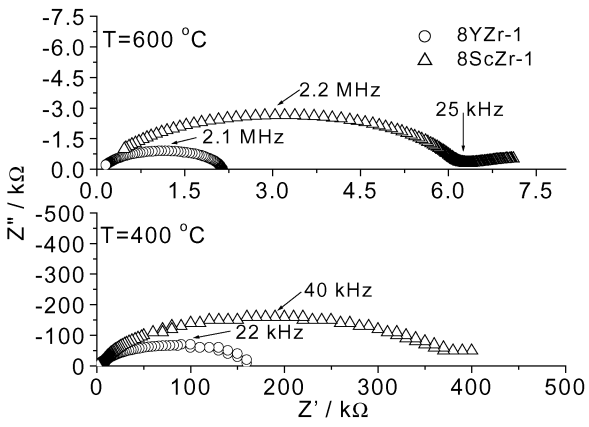

Fig. 12 Impedance spectra of nanocrystalline 8YZr-1 and 8ScZr-1 at 400 and 600 °C.

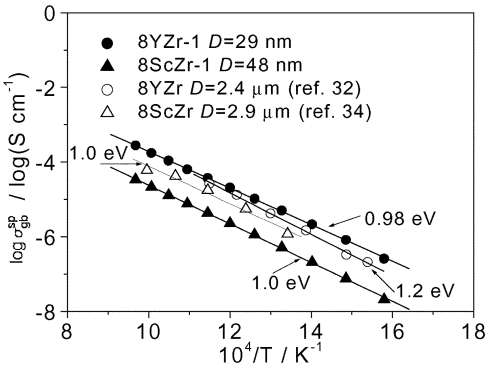

Fig. 13 Arrhenius plots of the specific grain boundary conductivity for the nanocrystalline 8YZr-1 and 8ScZr-1 and the corresponding microcrystalline materials.

(at high frequency), grain boundary resistance and electrode reaction impedance (at low frequency), are observed for the microcrystalline materials. At high temperature, the bulk resistance defines the electrical conductivity, though the high frequency semicircle is correlated with both the bulk and grain boundary resistance.[32]

Based on the brick layer model,[33] in the case that the specific grain boundary conductivity σ_{gb}^{sp} is identical in all the samples, the total grain boundary conductivity σ_{gb}^{T} should decease with decreasing grain size and is given by:

$$\sigma_{gb}^{T} = \sigma_{gb}^{sp} (D/\delta_{gb})$$

where D is the average grain size and δ_{gb} is the width of the grain boundary, which was assumed to be 2 nm in the ZrO_2 system.[32]

Fig. 13 shows an Arrhenius plot of the specific grain boundary conductivity for the 8YZr-1 and 8ScZr-1 samples. It can be seen that the conductivity activation energy for the grain boundary of nanocrystalline 8YZr-1 is 0.22 eV smaller than that of microcrystalline 8YZr. It can also be seen that the specific grain boundary conductivity values of nanocrystalline 8YZr-1 markedly increase, when compared with those of microcrystalline 8YZr, over the temperature range of 360–600 °C. Recently, Kosacki *et al.*[13] observed a decreased activation energy from 1.23 eV to 0.93 eV and an enhanced conductivity (about two orders of magnitude) for micro- (D = 2.4 μm) and nanocrystalline 8YZr (D = 20 nm). They attributed the electrical properties (defined by the grain boundary effect) of the nanocrystallite to the grain-size-dependent stoichiometry. Thus, here, the ionic conduction in nanocrystalline 8YZr-1 should be considered to be related to the size-dependent stoichiometry. On the other hand, the enhanced specific grain boundary conductivity could be explained by the size-dependent grain boundary impurity segregation (such as Si), as proposed by Aoki *et al.*[32] They proved that the reduced grain size can bring about a decreased amount of segregated Si at the grain boundaries and thus enhance the specific grain boundary conductivity.[32] Similar effects were also observed in nanocrystalline 8YZr,[13,14,34] 8ScZr,[14,34] and $SrCe_{0.95}Yb_{0.05}O_3$ (ref. 35) thin films, nanocrystalline $(Y_2O_3)_x(ZrO_2)_{1-x}$ (x = 0.017, 0.029),[36] TiO_2 (ref. 37) and CeO_2,[38] and microcrystalline $(CaO)_{0.15}(ZrO_2)_{0.85}$.[32]

In the case of 8ScZr-1 specimen, from Fig. 13, it can be seen that the conductivity activation energy for the grain boundary conductivity of the nanocrystallite is identical to that of the microcrystallite. But the specific grain boundary conductivity of the nanocrystallite is much lower than that of the microcrystallite. The source accounting for the difference in ionic conduction displayed by nanocrystalline 8YZr-1 and 8ScZr-1 is still confused and needs further clarification.

Conclusions

Homogeneous nanocrystalline $(ZrO_2)_{0.92}(RE_2O_3)_{0.08}$ (RE = Y, Sc) with large specific surface area of cubic structure were solvothermally synthesized from the urea coprecipitated (Zr,RE)-hydroxide gel or the gel-calcined oxide in water (or absolute ethanol) under mild conditions. Both the hydroxide and the oxide powders showed very high solvothermal reactivity. The heterogeneous nucleation-growth, *i.e.* an *in situ* transformation of hydrous (Zr,RE)-oxide with an ordered cubic structure *via* dissolution and recrystallization is proposed to be predominately responsible for the nanocrystalline crystallization. The as-obtained nanocrystallite exhibited a good sinterability. For grain boundary effect governs the ionic conduction in the nanosize range, one semicircle at high frequency could be observed in the impedance spectra of the nanocrystallite over the measurement temperature range of 360–800 °C. Nanocrystalline $(ZrO_2)_{0.92}(Y_2O_3)_{0.08}$ displayed enhanced specific grain boundary conductivity due to size-dependent grain boundary impurity segregation.

Acknowledgement

We gratefully acknowledge the financial aid from MOST (G1998061300), and NSFC (Nos. 20171003, 20023005 and 29831010).

References

1 H. Hahn, *Nanostruct. Mater.*, 1997, **9**, 3.
2 J. Grabis, A. Kuzjukevics, D. Rasmane, M. Mogensen and S. Linderoth, *J. Mater. Sci.*, 1998, **33**, 723.
3 F. L. Yuan, C. H. Chen, E. M. Kelder and J. Schoonman, *Solid State Ionics*, 1998, **109**, 119.
4 A. Tsoga, A. Naoumidis, W. Jungen and D. StoÈve, *J. Eur. Ceram. Soc.*, 1999, **19**, 907.
5 O. G. Ellert, I. A. Petrunenko, M. V. Tsodikov, O. V. Bukhtenko, D. I. Kochubey, Y. V. Maksimov, R. A. Dominguez, F. L. Cumbreras and J. A. Navio, *J. Sol-Gel Sci. Technol.*, 1997, **8**, 213.
6 M. Z. C. Hu, M. T. Harris and C. H. Byers, *J. Colloid Interface Sci.*, 1998, **198**, 87.
7 A. Cabanas, J. A. Darr, E. Lester and M. Poliakoff, *Chem. Commun.*, 2000, 901.
8 S. Somiya and T. Akiba, *J. Eur. Ceram. Soc.*, 1999, **19**, 81.
9 M. Yoshimura and S. Somiya, *Mater. Chem. Phys.*, 1999, **61**, 1.
10 J. D. Lin and J. G. Duh, *J. Am. Ceram. Soc.*, 1998, **81**, 853.
11 J. P. Zhao, W. H. Fan, D. Wu and Y. H. Sun, *J. Mater. Res.*, 2000, **15**, 402.
12 H. L. Tuller, *Solid State Ionics*, 2000, **131**, 143.
13 I. Kosacki, T. Suzuki, V. Petrovsky and H. U. Andersom, *Solid State Ionics*, 2000, **136–137**, 1225.
14 Y. W. Zhang, Y. Yang, S. Jin, S. J. Tian, G. B. Li, J. T. Jia, C. S. Liao and C. H. Yan, *Chem. Mater.*, 2001, **13**, 372.
15 J. D. Lin and J. G. Duh, *J. Am. Ceram. Soc.*, 1997, **80**, 92.
16 G. Dell'Agli and G. Mascolo, *J. Eur. Ceram. Soc.*, 2000, **20**, 139.
17 J. I. Langford, *J. Appl. Crystallogr.*, 1971, **4**, 259.
18 J. I. Langford, *J. Appl. Crystallogr.*, 1973, **6**, 190.
19 A. Guinier, in *Theorie et Technique de la Radiocristallographie*, Dunod, Paris, 3rd edn., 1964, p. 482.
20 J. E. Bauerle, *J. Phys. Chem. Solids*, 1969, **30**, 2657.
21 G. Xu, Y. W. Zhang, C. S. Liao and C. H. Yan, *Solid State Commun.*, 2002, **121**, 45.
22 M. Hirano and M. Inagaki, *J. Mater. Chem.*, 2000, **10**, 473.
23 Y. X. Huang and C. J. Guo, *Powder Technol.*, 1992, **72**, 101.
24 T. Tsukada, S. Venigalla, A. A. Morrone and J. H. Adair, *J. Am. Ceram. Soc.*, 1999, **82**, 1169.
25 C. F. J. Baes and R. E. Mesmer, in *The Hydrolysis of Cations*, Wiley, New York, 1976.
26 H. Nishizawa, N. Yamasaki, K. Matsuoka and H. Mitsushio, *J. Am. Ceram. Soc.*, 1982, **65**, 343.
27 G. Dell'Agli and G. Mascolo, *J. Eur. Ceram. Soc.*, 2001, **21**, 29.
28 P. Pinceloup, C. Courtois, J. Vicens, A. Leriche and B. Thierry, *J. Eur. Ceram. Soc.*, 1999, **19**, 973.
29 D. W. Strickler and W. G. Carlson, *J. Am. Ceram. Soc.*, 1965, **48**, 286.

30 H. G. Scott, *J. Mater. Sci.*, 1975, **10**, 1527.
31 J. T. S. Irvine, D. C. Sinclair and A. R. West, *Adv. Mater.*, 1990, **2**, 132.
32 M. Aoki, Y.-M. Chiang, I. Kosacki, J. L.-R. Lee, H. L. Tuller and Y. P. Liu, *J. Am. Ceram. Soc.*, 1996, **79**, 1169.
33 T. Van Dijk and A. J. Burggraaf, *Phys. Status Solidi A*, 1983, **63**, 229.
34 Y. W. Zhang, S. Jin, Y. Yang, G. B. Li, S. J. Tian, J. T. Jia, C. S. Liao and C. H. Yan, *Appl. Phys. Lett.*, 2000, **77**, 3409.
35 I. Kosacki and H. U. Anderson, *Appl. Phys. Lett.*, 1996, **69**, 4171.
36 P. Mondal, A. Klein, W. Jaegermann and H. Hahan, *Solid State Ionics*, 1999, **118**, 331.
37 C. Demetry and X. L. Shi, *Solid State Ionics*, 1999, **118**, 271.
38 Y.-M. Chiang, E. B. Lavik, I. Kosacki, H. L. Tuller and J. Y. Ying, *Appl. Phys. Lett.*, 1996, **69**, 185.